

## Voltage-controlled ferromagnetic order in MnGe quantum dots

This article has been downloaded from IOPscience. Please scroll down to see the full text article.

2010 Nanotechnology 21 375606

(<http://iopscience.iop.org/0957-4484/21/37/375606>)

View [the table of contents for this issue](#), or go to the [journal homepage](#) for more

Download details:

IP Address: 164.67.26.22

The article was downloaded on 20/08/2010 at 20:35

Please note that [terms and conditions apply](#).

# Voltage-controlled ferromagnetic order in MnGe quantum dots

Faxian Xiu<sup>1</sup>, Igor V Ovchinnikov, Pramey Upadhyaya, Kin Wong, Xufeng Kou, Yi Zhou and Kang L Wang

Department of Electrical Engineering, University of California at Los Angeles, Los Angeles, CA 90095-1594, USA

E-mail: [xiu@ee.ucla.edu](mailto:xiu@ee.ucla.edu), [iovchinnikov@ucla.edu](mailto:iovchinnikov@ucla.edu), [prameyu@ucla.edu](mailto:prameyu@ucla.edu), [kinwong@ee.ucla.edu](mailto:kinwong@ee.ucla.edu), [xufengkou@ucla.edu](mailto:xufengkou@ucla.edu), [yizhou@ee.ucla.edu](mailto:yizhou@ee.ucla.edu) and [wang@ee.ucla.edu](mailto:wang@ee.ucla.edu)

Received 12 May 2010, in final form 6 July 2010

Published 20 August 2010

Online at [stacks.iop.org/Nano/21/375606](http://stacks.iop.org/Nano/21/375606)

## Abstract

Here, we speculate that room temperature voltage-controlled ferromagnetic ordering may become a founding phenomenon for the next generation of low-power spintronics nanodevices and discuss the special role of dilute magnetic semiconductors as the most reliable material basis to date. Then, we report on our latest experimental achievements in the voltage manipulation of the ferromagnetism in MnGe quantum dots, experimentally demonstrating the capacity of pushing the Curie temperature further above room temperature for technological applications.

(Some figures in this article are in colour only in the electronic version)

## 1. Introduction

The recent challenges faced in scaling by complementary metal–oxide–semiconductor (CMOS) technology have prompted the search for alternative solutions, one of which is magneto-electronics (ME). The underlying idea is that ME devices use the electron spin instead of the electron charge as a state variable and/or memory unit. It is understood that in order to be competitive with CMOS, ME devices should be operable at room temperature (RT) and have solid-state realization. The above requirements exclude the implementation of spins of single electrons, thus promoting the usage of the ferromagnetic order (FO)—the collective electron spins of ferromagnetic materials. The FO of tiny metallic parts has been employed for magnetic data storage purposes for decades [1] with the most recent achievement in this direction being electric-current-controlled spin-transfer-torque (STT) memory [2–4]. FO-based memory is advantageous [5] in the light of the (inhomogeneous) variability issues of electron-charge-based memory.

As opposed to the purposes of data storage, in which the high variability is the most outstanding problem at the nanometer scale, information processing (or data manipulation) suffers mostly from energy dissipation issues.

The dissipation comes mainly from the electric currents controlling the operation of the device. From this perspective, the use of the FO in combination with electric-current control may deteriorate all the possible advantages of switching to the FO state variables. For example, STT cells, considered as state variables, will require electric currents too high for their manipulation [6], which would make such manipulation of data even more power consuming than conventional processors. Furthermore, the characteristic energy of the FO anisotropy is orders of magnitude lower than that of the electron band structure. As a result, it is very unlikely that the back-action of the FO can efficiently control the electric charge flow. This, in turn, makes unfeasible the ‘reverse’ idea of using the FO for the control of the electron current instead. The connotation of the above discussion is that it is likely necessary to master the control of the FO through the low-dissipative bias voltage in order to be able to make use of the FO as a state variable for computations.

One such possibility is the multiferroic materials, which in addition possess the ferroelectric order coupled to the FO. The spatial orientation of the FO is thus controllable in multiferroics through the voltage control of the ferroelectric order [7–10]. Another idea being developed lately is the possibility of voltage control of the very existence of the FO—voltage-controlled ferromagnetic ordering (VCFO). One of the possible (and in a sense ultimate) devices enabled by VCFO

<sup>1</sup> Author to whom any correspondence should be addressed.

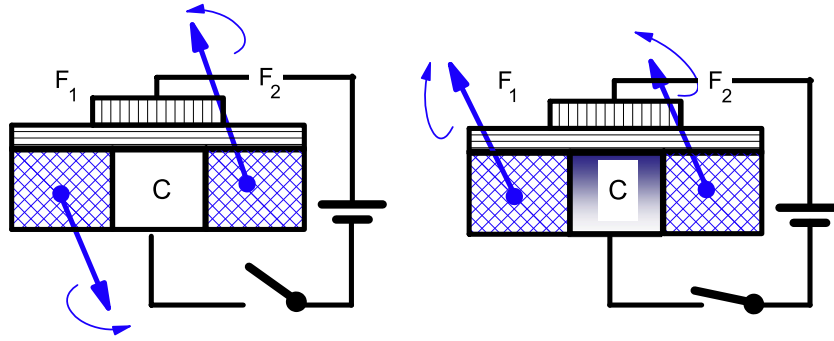


**Figure 1.** The instanton-transistor is a device with a controllable non-local exchange coupling between two ferromagnetic state variables, F1 and F2. The gate voltage turns the non-local exchange coupling between F1 and F2 on and off. When the channel is ‘off’ (left figure), F1 and F2 tend to align according to the magnetic dipole interaction between them. When the channel is ‘on’, the non-local exchange interaction through the channel tends to overcome the magnetic dipole interaction and align F1 and F2 in the same direction. The state of the device with F1 and F2 aligned in opposite directions can be viewed as though there is a domain wall (instanton) in the channel. Alternatively, the operation of the device can be viewed as a transistor, which controls the instanton-current between F1 and F2. From this perspective, F1 and F2 can be looked upon as the ‘source’ and ‘drain’ for the magnetic-orientation.

is what could be called an instanton-transistor. This device enables the gate-voltage control of the instanton-current flow (or the magnetization-orientation flow), that is of the non-local exchange coupling between the magnetization orientation of the ‘source’ and ‘drain’, as shown in figure 1. The physical essence of the operation of the VCFO-material-based instanton-channel is that its Curie temperature ( $T_c$ ) is close enough to the RT and the relative position of  $T_c$  and RT on the temperature scale can be reversibly interchanged by the gate voltage.

From a material realization point of view, on trying to locate the requirements which a VCFO material must satisfy, one expects that in reality the voltage variation of  $T_c$  is relatively small. This implies that the device operates in the critical region. In the critical region, the influence of the injected carriers on the magnetization is determined by the magnetic correlation length,  $\xi \sim \Lambda(T_c/|T - T_c|)^\nu$ , where  $\nu$  is the critical exponent, which depends on the universality class of ferromagnetic transition, and  $\Lambda$  is the so-called cutoff—a characteristic length, which is approximately several lattice constants and which does vary considerably for different materials. The correlation length diverges near the transition point and can definitely be in the order of dozens of nanometers in the critical region. The above is true for all ferromagnets and consequently for the nanometer-scale realization of the VCFO all ferromagnets with  $T_c$  close to RT are more or less the same [11–15]. From another point of view, the coupling between the FO and the injected carriers must be strong. Again, all the itinerant-electron ferromagnets (even metals) satisfy this requirement. Supporting the above statements is the recent experimental demonstration of that in complex oxides, in which electron density is almost at the metallic level ( $10^{21} \text{ cm}^{-3}$ ), the  $T_c$ -variation is even higher than that in (Mn)GaAs DMS [16]. Nevertheless, due to their high compatibility of DMS with today’s Si technology, it is likely that the reliable RT-VCFO will be first realized in the DMS materials.

Among the DMSs are Mn-doped Si and Ge, which have attracted extensive attention recently [17–27]. In these

materials, both the  $T_c$  and the saturation magnetization depend on the interplay of a variety of factors, which are ultimately determined by the growth conditions and post-annealing process [28, 29]. The concentration and distribution of Mn dopants, the carrier density, the presence of common defects such as Mn interstitials and Mn clusters significantly influence the magnitude and interactions of the magnetic coupling [26–30]. It is anticipated that this interplay between various growth parameters can be reduced in low dimensional structures [31]. In addition, nanostructures such as Mn-doped Ge quantum dots (QDs) could offer unique and salient physical properties, arising from size-related quantum confinement effects, and affect the carrier transport, spin-coherence lifetime, interactions between spins, and thus the ferromagnetic properties in general [32]. More importantly, the magnetic  $\text{Mn}_x\text{Ge}_{1-x}$  can be directly incorporated with the current CMOS platforms, promoting immediate applications in the microelectronics industry.

The first demonstration of VCFO was that in (In, Mn)As materials, in which the  $T_c$  was varied by  $\pm 1 \text{ K}$  with a voltage of  $\pm 125 \text{ V}$ , corresponding to an electric field of approximately  $\pm 1.6 \text{ MV cm}^{-1}$  [16]. The applicability of this phenomenon, however, is limited because of the low  $T_c$  of (In, Mn)As [33]. On the other hand, Mn-doped Ge DMS was reported to possess a much higher  $T_c$ s. For example, in  $\text{Mn}_{0.06}\text{Ge}_{0.94}$  single-crystalline thin films [34],  $T_c \sim 285 \text{ K}$ . In other experimental studies, the magnetic properties of  $\text{Mn}_x\text{Ge}_{1-x}$  nanostructures were carried out by the ion implantation of Mn [35]. The signature of the influence of the injected carriers on the ferromagnetic properties of  $\text{Mn}_x\text{Ge}_{1-x}$  nanostructures was observed by applying gate biases in MOS capacitors at a low temperature of 10 K. However, the existence of metallic precipitates such as  $\text{Mn}_5\text{Ge}_3$  and  $\text{Mn}_{11}\text{Ge}_8$  in these nanostructures, was expected to partly jeopardize the voltage-controlled hole-mediated exchange coupling. In this paper, we continue our previous work [35, 36], and demonstrate by structural and magnetic characterizations the successful fabrication of the single-crystalline DMS QDs without signatures of the  $\text{Mn}_5\text{Ge}_3$  or  $\text{Mn}_{11}\text{Ge}_8$  precipitates.

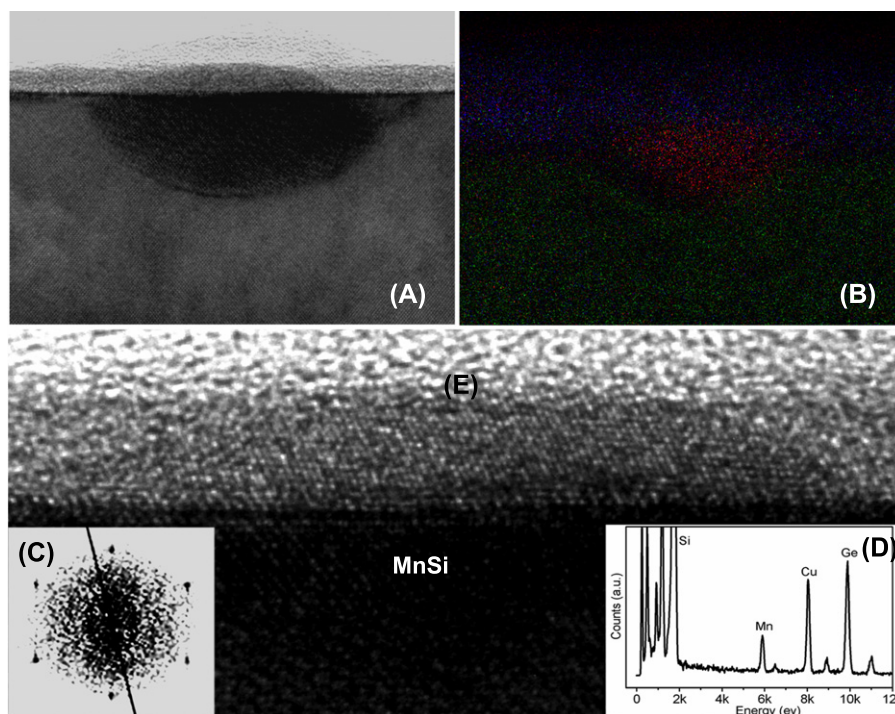


**Figure 2.** The structural properties of  $\text{Mn}_{0.05}\text{Ge}_{0.95}$  QDs grown on a p-type Si substrate. (A) A high-resolution TEM (HR TEM) cross-section image of a  $\text{Mn}_{0.05}\text{Ge}_{0.95}$  QD. Mn diffuses into the Si substrate, which is shown directly underneath the  $\text{Mn}_{0.05}\text{Ge}_{0.95}$  QD. (B) The EELS composition mapping of Mn distribution. (C) The corresponding SAED pattern of  $\text{Mn}_{0.05}\text{Ge}_{0.95}$  QD, revealing a single-crystalline structure. (D) An EDS composition spectrum showing that both Mn and Ge are present in  $\text{Mn}_{0.05}\text{Ge}_{0.95}$  QD. (E) An enlarged HR TEM image to show the detailed lattice structure of  $\text{Mn}_{0.05}\text{Ge}_{0.95}$  QD.

We investigate the  $T_c$  of the material by a superconducting quantum interference device (SQUID) magnetometer, and find that  $T_c$ , in principle, could be as high as 400 K. These high  $T_c$ s can be attributed to the quantum confinement of the carriers in the QD geometry, as confirmed by the numerical studies also presented in the paper. Further, we investigate the influence of the gate bias on the ferromagnetic properties of the  $\text{Mn}_{0.05}\text{Ge}_{0.95}$  DMS QDs up to 100 K. The measurements at higher temperatures (closer to the  $T_c$ ) have not been realized yet due to leakage current limitations. Nevertheless, even away from the transition, we were able to see the influence of the gate bias on the magnetic properties. The main aim of the present work is to provide a theoretical understanding of the high Curie temperature nature of these quantum dots, which also explains the gate modulated ferromagnetism.

## 2. Results and discussion

### 2.1. Fabrication

MnGe QDs were produced on p-type Si substrates by a solid-source MBE system. The Mn and Ge sources were provided by traditional effusion cells. The self-assembled MnGe QDs were grown at 450 °C with a Ge growth rate of 0.2 Å s<sup>-1</sup>, similar to the growth of pure Ge QDs on Si under a typical Stranski–Krastanov (SK) mode. The MOS capacitors were fabricated by depositing 40 nm thick Al<sub>2</sub>O<sub>3</sub> on top of the  $\text{Mn}_{0.05}\text{Ge}_{0.95}$  QD layer at 250 °C via an atomic layer deposition technique. The front and back sides were metallized with 200 nm thick Au as

the contact electrodes. The MOS capacitors were loaded into the SQUID magnetometer for bias-dependent magnetization measurements at different temperatures. We have noted that the quality of the dielectric layer is very critical to minimize the leakage current. A thick Al<sub>2</sub>O<sub>3</sub> of 40 nm ensures a relatively small leakage current below 10<sup>-6</sup> A cm<sup>-2</sup>.

### 2.2. Structural properties of $\text{Mn}_{0.05}\text{Ge}_{0.95}$ QDs

Cross-section TEM was carried out to determine the structural characteristics and the Mn composition of the  $\text{Mn}_{0.05}\text{Ge}_{0.95}$  QDs. It reveals a dome-shaped dot on top of the Si substrate with a Mn diffusion area underneath as shown in figure 2(A). The dots have a typical base diameter of about 30 nm and a height of about 8 nm. Electron energy loss spectroscopy (EELS) shows that Mn dopants distribute uniformly inside the dots (figure 2(B)). A selected area electron diffraction pattern (SAED) reveals a single-crystalline system (figure 2(C)). The interface between the dot and the Si substrate shows excellent lattice coherence without pronounced dislocations or stacking faults (figure 2(E)). Energy dispersive x-ray spectroscopy (EDS) confirms further the presence of Mn and Ge inside the dots. Based on an extensive composition analysis over many QDs, the percentage of Mn was determined to be about 5% and no metallic phases, such as Mn<sub>5</sub>Ge<sub>3</sub> and Mn<sub>11</sub>Ge<sub>8</sub>, were found. However, due to the extensive Mn doping, the formation of Mn clusters which are beyond the detection limit of conventional TEM cannot be completely excluded.

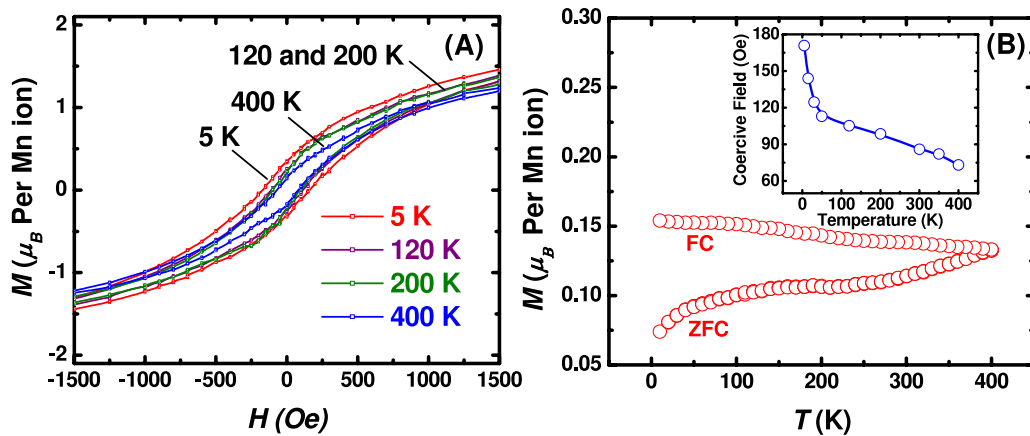


**Figure 3.** Magnetic properties of the  $\text{Mn}_{0.05}\text{Ge}_{0.95}$  QDs grown on a p-type Si substrate. (A) Hysteresis loops measured at different temperatures from 5 to 400 K. The observation of a hysteresis loop at 400 K indicates a strong ferromagnetism above room temperature. (B) Zero field cooled and field cooled magnetizations of QDs with a magnetic field of 100 Oe; the inset shows the coercivity values at different temperatures.

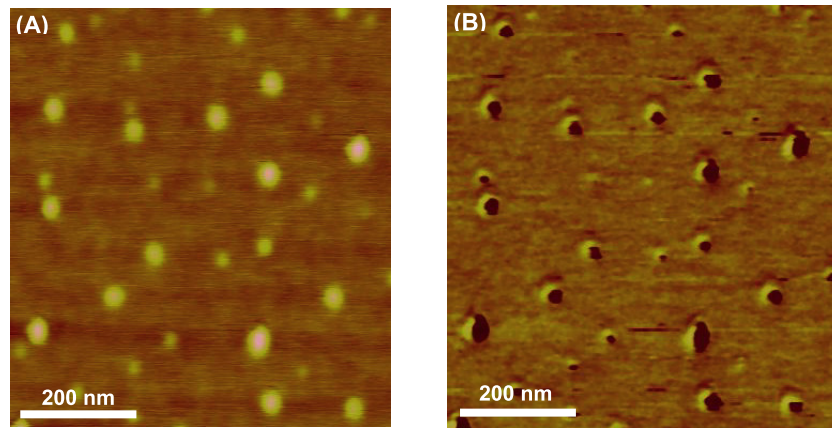


**Figure 4.** AFM and MFM images of the  $\text{Mn}_{0.05}\text{Ge}_{0.95}$  QDs measured at 320 K. (A) Typical AFM image of  $\text{Mn}_{0.05}\text{Ge}_{0.95}$  QDs. (B) Corresponding MFM image.  $\text{Mn}_5\text{Ge}_3$  and  $\text{Mn}_{11}\text{Ge}_8$  can be excluded because of their low Curie temperatures of 296–300 K.

### 2.3. Magnetic properties of $\text{Mn}_{0.05}\text{Ge}_{0.95}$ QDs

The magnetic properties were carried out using a SQUID system. Figure 3(A) shows temperature-dependent hysteresis loops when the external magnetic field is parallel to the sample surface (in-plane). The field-dependent magnetization indicates a strong ferromagnetism above 400 K. The saturation magnetic moment per Mn atom is estimated to be  $1.8 \mu_B$  at 5 K. A fraction of roughly 60% of Mn is estimated to be activated assuming that each Mn has a moment of  $3 \mu_B$  [18, 37–39]. Zero field cooled (ZFC) and field cooled (FC) magnetizations were measured with a magnetic field of 100 Oe as shown in figure 3(B). The magnetic moments do not drop to zero, suggesting a high  $T_c$  beyond 400 K. From these two curves, one can also infer the formation of a single phase in this material system, i.e., DMS QDs, which is surprisingly similar to the high  $T_c$  DMS  $\text{Mn}_{0.05}\text{Ge}_{0.95}$  nanowires [40]. The wide separation of the ZFC and FC curves in the temperature range of 5–400 K shows the irreversibility of susceptibilities, possibly arising from strain-induced anisotropy since a large lattice mismatch exists between Si and Ge [41]. The temperature-dependent coercivity is shown in figure 3(B)

inset. Similar to the  $\text{Mn}_x\text{Ge}_{1-x}$  nanowires [42], the coercivity decreases from 170 Oe (at 5 K) to 73 Oe (at 400 K). The small coercivity in the entire temperature range measured features a soft ferromagnetism which originates from Mn ions diluted in the Ge matrix [43]. The above magnetic properties support the fact that the  $\text{Mn}_{0.05}\text{Ge}_{0.95}$  QDs exhibit a DMS-type ferromagnetic order.

Atomic force microscopy (AFM) and magnetic force microscopy (MFM) measurements were carried out to investigate the morphology and ferromagnetism of the  $\text{Mn}_{0.05}\text{Ge}_{0.95}$  QDs at 320 K, respectively. The average dot size is about 50 nm in base diameter and 6 nm in height. The dot density is about  $6 \times 10^9 \text{ cm}^{-2}$  (figure 4(A)). The corresponding MFM image was taken by lifting up the MFM probe 25 nm above the topographic height of the sample in a phase detection mode (figure 4(B)). The appearance of bright-and-dark areas in the MFM image clearly shows the formation of magnetic domains in the  $\text{Mn}_{0.05}\text{Ge}_{0.95}$  QDs, which is similar to (In, Mn)As DMS QDs [44]. Since the experiments were performed at 320 K, the formation of metallic phases such as  $\text{Mn}_5\text{Ge}_3$  and  $\text{Mn}_{11}\text{Ge}_8$  can be easily ruled out because they have a low  $T_c$  of 296–300 K [29]. Overall, the above MFM results agree well

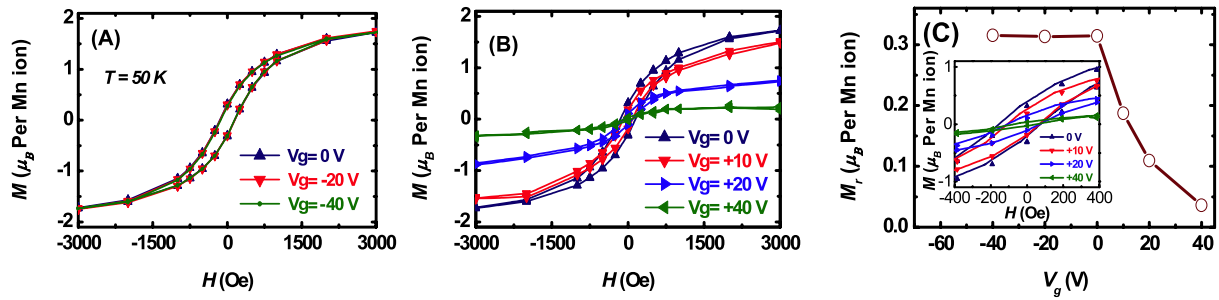


**Figure 5.** The manipulation of ferromagnetism of MnGe QDs by applying electrical fields. (A) Hysteresis loops with zero and negative bias of  $-20$  and  $-40$  V on the gate. (B) The hysteresis loops with zero and positive bias of  $+10$ ,  $+20$ , and  $+40$  V. (C) A representation of remnant moments with respect to the gate bias. Inset is the enlarged figure for the central part of (B) to clearly show the change of remnant moment. It is found that the remnant moments can be manipulated by applying bias on the MOS gate. The saturation moments can be also manipulated by the gate bias.

with the TEM observations and the ferromagnetic order at high temperatures obtained in the SQUID measurements.

#### 2.4. Voltage-controlled ferromagnetic ordering

Figures 5(A) and (B) show the hysteresis loops by SQUID with negative and positive biases on the MOS gate at 50 K, respectively. Under a negative bias, the holes are attracted into the channel of the device (accumulation). In this circumstance, however, the hysteresis loop does not show a remarkable change (figure 5(A)). This could be explained by the fact that even at 0 V, the QD device is already accumulated with enough holes to induce ferromagnetism. In other words, the hole-mediated effect is sufficient to align a majority of the activated Mn ions along one direction in each individual QD. Further increasing the negative bias does not change the hole concentrations much.

On the contrary, with the positive bias, a large amount of holes are depleted into the p-type Si so that the hole-mediated effect is notably reduced. As a result, the Mn ions start to misalign because of the lack of holes. The saturation moment per Mn ion decreases more than ten times as the gate bias increases from 0 to  $+40$  V (figure 5(B)). It should be noted that, at  $+40$  V, the saturation and remnant moments of the  $\text{Mn}_{0.05}\text{Ge}_{0.95}$  QDs become fairly weak, resembling a ‘paramagnetic-like’ state. Figure 5(C) summarizes the change of remnant moments as a function of gate voltage. The inset in figure 5(C) displays an enlarged picture to clearly show the change of remnant moments with respect to the gate bias. The above results evidently demonstrate that the hole-mediated effect does exist in this material system, which is also supported by our previous experiments [35].

The desired high concentration of electrons on the surface, needed to deplete the DMS, is limited in our case solely by the leakage current. This is, in fact, the reason why we studied the voltage effect well below the ferromagnetic transition, which is expected to be somewhere around  $\sim 400$  K, as implied by our SQUID measurements (see section 2.3). By increasing the measurement temperature to 100 K (not shown here), the modulation of the ferromagnetism turned out to be less pronounced compared to that at 50 K, which we believe is due to the increased leakage current in our MOS devices.

#### 2.5. Role of the quantum confinement: numerical results

The fact that Curie temperatures in nanostructures [42, 44, 45] are typically higher than in the bulk materials can be attributed to the effects of quantum confinement [46]. To demonstrate this in our case of MnGe QDs, we performed first-principle calculations comparing the electronic structure of the bulk  $\text{Mn}_{0.06}\text{Ge}_{0.94}$  and small MnGe QDs (diameter  $\sim 9$  Å).

The bulk  $\text{Mn}_{0.06}\text{Ge}_{0.94}$  system was simulated within local spin-density approximation (LSDA) to density functional theory using the periodic boundary condition. The kinetic energy cutoff used for the wavefunctions was 280 eV. The simulated supercell contained 16 atoms at the experimental Ge lattice constant ( $a = 5.6$  Å) with the central atom replaced by Mn (corresponding to the case of a substitutional impurity, see figure 6(B)). The other extreme of  $\text{Mn}_1\text{Ge}_{28}\text{H}_{36}$  (diameter  $\sim 9$  Å) QD was also simulated within LSDA to density functional theory using the confined boundary condition (i.e. real-space wavefunctions going to zero outside a sphere enclosing the quantum dot). The structure of the QD was constructed by taking a spherical fragment of the corresponding bulk diamond structure of Ge with the surface passivated by hydrogen atoms and the central atom replaced by Mn (figure 7(B)). The surface was passivated to get rid of the surface states (introduced by dangling bonds at the surface) in the band gap [46]. The radius of the sphere enclosing this dot (outside which wavefunctions go to zero) and the grid spacing were varied until the corresponding eigenvalues converged. These values were 10 and 0.15 Å for the radius of the enclosing sphere and grid spacing respectively.

The calculated total and d-like impurity density of states (DOS) for bulk shows d-like impurity states lying well below the Fermi-level (indicated by dashed vertical line in figure 6(A)). This location of impurity states in turn implies that the carriers (holes at the Fermi-level) have more p-like character of the host Ge because of less mixing (hybridization) with the d-like Mn impurity states. The expected effect of quantum confinement on the DOS is to move these impurity states towards the Fermi-level (as indicated by arrows in figure 6(A)) [46, 47] and hence increase the hybridization between the carriers (holes at the Fermi-level) and impurity states. This increase in hybridization between carriers

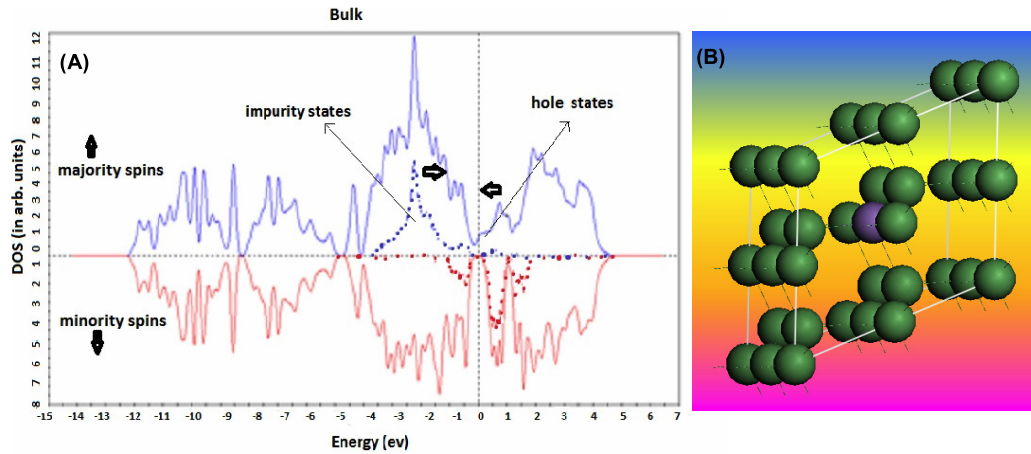


**Figure 6.** (A) The total density of states (solid curve) and the DOS of the impurity levels (dashed curve) in bulk  $\text{Mn}_{0.06}\text{Ge}_{0.94}$  as found using the CASTEP [48] are given. As one goes to nanometer sizes, the density of state of the localized d-like impurities and the itinerant p-like carriers are expected (see next figure) to move toward each other on the energy scale, as indicated by the black arrows. (B) Simulated supercell structure.

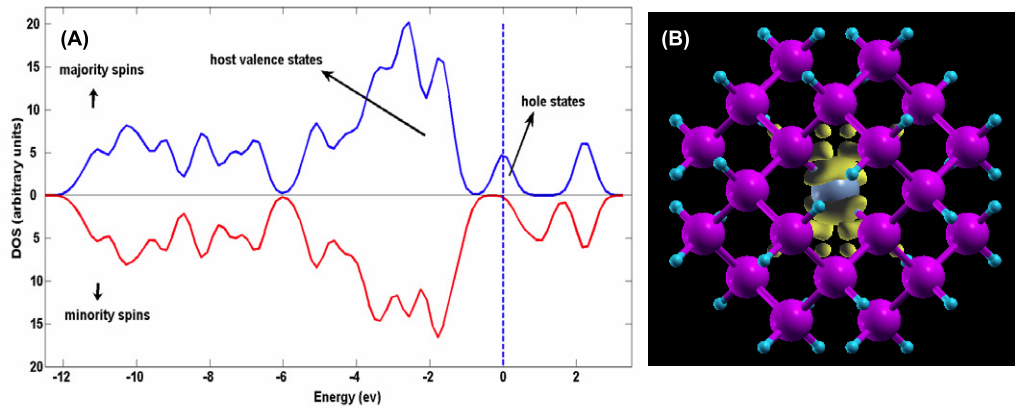


**Figure 7.** The demonstration of the effect of quantum confinement on the carrier localization (using PARSEC [49]). (A) DOS of  $\text{Ge}_{28}\text{Mn}_1\text{H}_{36}$  (diameter  $\sim 9 \text{ \AA}$ ), the p-like holes are trapped on the impurity d-like states and are detached from the host valence band. (B) The yellow surface represents the typical isosurface of the hole wavefunction squared showing the localized character of the holes around the only impurity in the cluster (central blue atom).

and impurity states would in turn lead to an increase in Curie temperature,  $T_c$  within the free-carrier mediated picture of the FO initially [46]. On the other hand  $T_c$  cannot increase monotonically with decreasing size as the increase in hybridization should also reduce the moving ability of the carriers making them more localized, thus, in turn, leading to the reduction of the effective exchange coupling between the neighboring magnetic dopants. Our numerical results for the limit of very small QD (diameter  $\sim 9 \text{ \AA}$ ) confirm this increase in hybridization and the corresponding increase in the localization of the carriers. Figure 7(A) shows that the holes and the impurity states both overlap and are detached from the Ge valence bands lying at the Fermi-level, thus assuming strong hybridization and the absence of hole mobility. This is further confirmed by the analysis of the spatial form of the hole wavefunctions near the Fermi-level (figure 7(A)).

The above picture implies that there must be a region of intermediate sizes (and possibly shapes), where the  $T_c$  should peak.

### 3. Conclusions

In summary, we discussed the technological importance of the possibility to control ferromagnetic state by low-dissipation bias voltages, and the important role of dilute magnetic semiconductors as the most likely candidates for the realization of this phenomenon. We presented our recent experimental achievements on the voltage control of the ferromagnetic properties of single-crystalline  $\text{Mn}_{0.05}\text{Ge}_{0.95}$  self-assembled QDs, grown on an Si substrate by the MBE. Using superconducting a quantum interference device magnetometer we found that  $T_c$  can in principle be as high as 400 K. We were able to investigate the influence of the gate bias on the ferromagnetic properties of the  $\text{Mn}_{0.05}\text{Ge}_{0.95}$  DMS QDs at temperatures up to 100 K—the limitation imposed by the thermo-activated leakage current. In combination with the numerical studies of DOS in this DMS, our experiments suggest that efficient voltage-controlled

ferromagnetic ordering at room temperature can be realized in this material.

## Acknowledgments

We gratefully acknowledge the financial support of the Western Institute of Nanoelectronics (WIN) and the Intel Spin-Gain FET project. We also thank our Australian collaborators Professor Jin Zou and Dr Yong Wang for their significant contributions of TEM experiments.

## References

- [1] Chappert C, Fert A and Van Dau F N 2007 The emergence of spin electronics in data storage *Nat. Mater.* **6** 813–23
- [2] Krivorotov I N, Emley N C, Sankey J C, Kiselev S I, Ralph D C and Buhrman R A 2005 Time-domain measurements of nanomagnet dynamics driven by spin-transfer torques *Science* **307** 228–31
- [3] Krivorotov I N, Emley N C, Garcia A G F, Sankey J C, Kiselev S I, Ralph D C and Buhrman R A 2004 Temperature dependence of spin-transfer-induced switching of nanomagnets *Phys. Rev. Lett.* **93** 166603
- [4] Kiselev S I, Sankey J C, Krivorotov I N, Emley N C, Rinkoski M, Perez C, Buhrman R A and Ralph D C 2004 Current-induced nanomagnet dynamics for magnetic fields perpendicular to the sample plane *Phys. Rev. Lett.* **93** 036601
- [5] Ovchinnikov I V and Wang K L 2008 Variability of electronics and spintronics nanoscale devices *Appl. Phys. Lett.* **92** 093503
- [6] Albert F J, Katine J A, Buhrman R A and Ralph D C 2000 Spin-polarized current switching of a Co thin film nanomagnet *Appl. Phys. Lett.* **77** 3809–11
- [7] Seidel J *et al* 2009 Conduction at domain walls in oxide multiferroics *Nat. Mater.* **8** 229–34
- [8] Martin L, Crane S P, Chu Y H, Holcomb M B, Gajek M, Huijben M, Yang C H, Balke N and Ramesh R 2008 Multiferroics and magnetoelectrics: thin films and nanostructures *J. Phys.: Condens. Matter* **20** 434220
- [9] Chu Y H *et al* 2008 Electric-field control of local ferromagnetism using a magnetoelectric multiferroic (vol 7, pg 478, 2008) *Nat. Mater.* **7** 678
- [10] Chu Y H *et al* 2006 Nanoscale domain control in multiferroic BiFeO<sub>3</sub> thin films *Adv. Mater.* **18** 2307
- [11] Ovchinnikov I V and Wang K L 2008 Voltage-controlled surface magnetization of itinerant ferromagnet Ni<sub>1-x</sub>Cu<sub>x</sub> *Phys. Rev. B* **78** 012405
- [12] Ovchinnikov I V and Wang K L 2009 Voltage sensitivity of Curie temperature in ultrathin metallic films *Phys. Rev. B* **80** 012405
- [13] Ovchinnikov I V and Wang K L 2009 Theory of electric-field-controlled surface ferromagnetic transition in metals *Phys. Rev. B* **79** 020402
- [14] Sun Y, Burton J D and Tsymal E Y 2010 Electrically driven magnetism on a Pd thin film *Phys. Rev. B* **81** 064413
- [15] Burton J D and Tsymal E Y 2009 Prediction of electrically induced magnetic reconstruction at the manganese/ferroelectric interface *Phys. Rev. B* **80** 174406
- [16] Ohno H, Chiba D, Matsukura F, Omiya T, Abe E, Dietl T, Ohno Y and Ohtani K 2000 Electric-field control of ferromagnetism *Nature* **408** 944–6
- [17] Bolduc M, Awo-Affouda C, Stollenwerk A, Huang M B, Ramos F G, Agnello G and LaBella V P 2005 Above room temperature ferromagnetism in Mn-ion implanted Si *Phys. Rev. B* **71** 033302
- [18] Park Y D, Hanbicki A T, Erwin S C, Hellberg C S, Sullivan J M, Mattson J E, Ambrose T F, Wilson A, Spanos G and Jonker B T 2002 A group-IV ferromagnetic semiconductor: Mn<sub>x</sub>Ge<sub>1-x</sub> *Science* **295** 651–4
- [19] Kang J S *et al* 2005 Spatial chemical inhomogeneity and local electronic structure of Mn-doped Ge ferromagnetic semiconductors *Phys. Rev. Lett.* **94** 147202
- [20] Passacantando M, Ottaviano L, D'Orazio F, Lucari F, Biase M D, Impellizzeri G and Priolo F 2006 Growth of ferromagnetic nanoparticles in a diluted magnetic semiconductor obtained by Mn<sup>+</sup> implantation on Ge single crystals *Phys. Rev. B* **73** 195207
- [21] Pinto N, Morresi L, Ficcadenti M, Murri R, D'Orazio F, Lucari F, Boarino L and Amato G 2005 Magnetic and electronic transport percolation in epitaxial Ge<sub>1-x</sub>Mn<sub>x</sub> films *Phys. Rev. B* **72** 165203
- [22] Wang Y, Zou J, Zhao Z, Han X, Zhou X and Wang K L 2008 Mn behavior in Ge<sub>0.96</sub>Mn<sub>0.04</sub> magnetic thin films grown on Si *J. Appl. Phys.* **103** 066104
- [23] Yoon I T, Lee S W, Kang T W, Koh D and Fu D J 2008 Ferromagnetic properties of Mn-implanted Ge/Si quantum dots *J. Electrochem. Soc.* **155** K1–4
- [24] Li A P, Wendelken J F, Shen J, Feldman L C, Thompson J R and Weitering H H 2005 Magnetism in Mn<sub>x</sub>Ge<sub>1-x</sub> semiconductors mediated by impurity band carriers *Phys. Rev. B* **72** 195205
- [25] Ahlers S, Bougeard D, Sircar N, Abstreiter G, Trampert A, Opel M and Gross R 2006 Magnetic and structural properties of Ge<sub>x</sub>Mn<sub>1-x</sub> films: precipitation of intermetallic nanomagnets *Phys. Rev. B* **74** 214411
- [26] Bihler C, Jaeger C, Vallaitis T, Gjukic M, Brandt M S, Pippel E, Woltersdorf J and Gosele U 2006 Structural and magnetic properties of Mn<sub>5</sub>Ge<sub>3</sub> clusters in a dilute magnetic germanium matrix *Appl. Phys. Lett.* **88** 112506
- [27] De Padova P *et al* 2008 Mn<sub>0.06</sub>Ge<sub>0.94</sub> diluted magnetic semiconductor epitaxially grown on Ge(001): influence of Mn<sub>5</sub>Ge<sub>3</sub> nanoscopic clusters on the electronic and magnetic properties *Phys. Rev. B* **77** 045203
- [28] Bolduc M, Awo-Affouda C, Ramos F and LaBella V P 2006 Annealing temperature effects on the structure of ferromagnetic Mn-implanted Si *J. Vac. Sci. Technol. A* **24** 1648–51
- [29] Jamet M *et al* 2006 High-Curie-temperature ferromagnetism in self-organized Ge<sub>1-x</sub>Mn<sub>x</sub> nanocolumns *Nat. Mater.* **5** 653–9
- [30] Biegger E, Staheli L, Fonin M, Rudiger U and Dedkov Y S 2007 Intrinsic ferromagnetism versus phase segregation in Mn-doped Ge *J. Appl. Phys.* **101** 103912
- [31] Brunner K 2002 Si/Ge nanostructures *Rep. Prog. Phys.* **65** 27–72
- [32] Knobel R, Samarth N, Crooker S A and Awschalom D D 2000 Spin-polarized quantum transport and magnetic field-dependent carrier density in magnetic two-dimensional electron gases *Physica E* **6** 786–9
- [33] Weisheit M, Fahler S, Marty A, Souche Y, Poinignon C and Givord D 2007 Electric field-induced modification of magnetism in thin-film ferromagnets *Science* **315** 349–51
- [34] Cho S, Choi S, Hong S C, Kim Y, Ketterson J B, Kim B-J, Kim Y C and Jung J-H 2002 Ferromagnetism in Mn-doped Ge *Phys. Rev. B* **66** 033303
- [35] Chen J, Wang K L and Galatsis K 2007 Electrical field control magnetic phase transition in nanostructured Mn<sub>x</sub>Ge<sub>1-x</sub> *Appl. Phys. Lett.* **90** 012501
- [36] Xiu F, Wang Y, Kim J, Hong A, Tang J, Jacob A P, Zou J and Wang K L 2010 Electric-field-controlled ferromagnetism in high-Curie-temperature Mn<sub>0.05</sub>Ge<sub>0.95</sub> quantum dots *Nat. Mater.* **9** 337–44
- [37] Stroppa A, Picozzi S, Continenza A and Freeman A J 2003 Electronic structure and ferromagnetism of Mn-doped group-IV semiconductors *Phys. Rev. B* **68** 155203



- [38] Schulthess T C and Butler W H 2001 Electronic structure and magnetic interactions in Mn doped semiconductors *J. Appl. Phys.* **89** 7021–3
- [39] Schilfgaard M V and Mryasov O N 2001 Anomalous exchange interactions in III–V dilute magnetic semiconductors *Phys. Rev. B* **63** 233205
- [40] Cho Y J, Kim C H, Kim H S, Lee W S, Park S-H, Park J, Bae S Y, Kim B, Lee H and Kim J-Y 2008 Ferromagnetic  $\text{Ge}_{1-x}\text{Mn}_x$  ( $M = \text{Mn, Fe, and Co}$ ) nanowires *Chem. Mater.* **20** 4694–702
- [41] Dietl T, Ohno H and Matsukura F 2001 Hole-mediated ferromagnetism in tetrahedrally coordinated semiconductors *Phys. Rev. B* **63** 195205
- [42] van der Meulen M I, Petkov N, Morris M A, Kazakova O, Han X, Wang K L, Jacob A P and Holmes J D 2008 Single crystalline  $\text{Ge}_{1-x}\text{Mn}_x$  nanowires as building blocks for nanoelectronics *Nano Lett.* **9** 50–6
- [43] Kazakova O, Kulkarni J S, Holmes J D and Demokritov S O 2005 Room-temperature ferromagnetism in  $\text{Ge}_{1-x}\text{Mn}_x$  nanowires *Phys. Rev. B* **72** 094415
- [44] Jeon H C, Jeong Y S, Kang T W, Kim T W, Chung K J, Jhe W and Song S A 2002  $(\text{In}_{1-x}\text{Mn}_x)\text{As}$  diluted magnetic semiconductor quantum dots with above room temperature ferromagnetic transition *Adv. Mater.* **14** 1725–8
- [45] Zheng Y H, Zhao J H, Bi J F, Wang W Z, Ji Y, Wu X G and Xia J B 2007 Cr-doped InAs self-organized diluted magnetic quantum dots with room-temperature ferromagnetism *Chin. Phys. Lett.* **24** 2118–21
- [46] Sapra S, Sarma D D, Sanvito S and Hill N A 2002 Influence of quantum confinement on the electronic and magnetic properties of  $(\text{Ga, Mn})\text{As}$  diluted magnetic semiconductor *Nano Lett.* **2** 605–8
- [47] Huang X, Makmal A, Chelikowsky J R and Kronik L 2005 Size-dependent spintronic properties of dilute magnetic semiconductor nanocrystals *Phys. Rev. Lett.* **94** 236801
- [48] Segall M D, Lindan P J D, Robert M J, Pickard C J, Hasnip D J, Clark S J and Payne M C 2002 First principles simulation: ideas, illustration and the CASTEP code *J. Phys.: Condens. Matter* **14** 2717
- [49] Chelikowsky J R, Troullier N and Saad Y 1994 Finite-difference-pseudopotential method: electronic structure calculations without a basis *Phys. Rev. Lett.* **72** 1240